A combinatorial approach to the repertoire of RNA kissing motifs; towards multiplex detection by switching hairpin aptamers

Guillaume Durand[1,2,3], Eric Dausse[1,2,3], Emma Goux[4], Emmanuelle Fiore[4], Eric Peyrin[4], Corinne Ravelet[4] and Jean-Jacques Toulmé[1,2,3,*]

[1]University of Bordeaux, ARNA Laboratory, 146 rue Léo Saignat, 33076 Bordeaux, France, [2]Inserm U1212, 146 rue Léo Saignat, 33076 Bordeaux, France, [3]CNRS UMR5320, 146 rue Léo Saignat, 33076 Bordeaux, France and [4]University Grenoble Alpes, Département de Pharmacochimie Moléculaire, CNRS UMR5063, 38400 St Martin d'Hères, France

ABSTRACT

Loop–loop (also known as kissing) interactions between RNA hairpins are involved in several mechanisms in both prokaryotes and eukaryotes such as the regulation of the plasmid copy number or the dimerization of retroviral genomes. The stability of kissing complexes relies on loop parameters (base composition, sequence and size) and base combination at the loop–loop helix - stem junctions. In order to identify kissing partners that could be used as regulatory elements or building blocks of RNA scaffolds, we analysed a pool of 5.2×10^6 RNA hairpins with randomized loops. We identified more than 50 pairs of kissing RNA hairpins. Two kissing motifs, 5'CCNY and 5'RYRY, generate highly stable complexes with K_Ds in the low nanomolar range. Such motifs were introduced in the apical loop of hairpin aptamers that switch between unfolded and folded state upon binding to their cognate target molecule, hence their name aptaswitch. The aptaswitch–ligand complex is specifically recognized by a second RNA hairpin named aptakiss through loop–loop interaction. Taking advantage of our kissing motif repertoire we engineered aptaswitch–aptakiss modules for purine derivatives, namely adenosine, GTP and theophylline and demonstrated that these molecules can be specifically and simultaneously detected by surface plasmon resonance or by fluorescence anisotropy.

INTRODUCTION

RNA hairpins offer a rich potential for intra- or intermolecular interactions with other RNA modules, thus generating tertiary and quaternary functional scaffolds. Complexes involving a few Watson–Crick base pairs between RNA loops have been demonstrated to control a number of biological functions. 'Hand-by-hand' interactions between apical and central loops were shown to take place in the dimerization of the bicoid mRNA required for the correct antero-posterior polarity of the drosophila embryo (1) as well as in the assembly of the pRNA of the *Bacillus subtilis* phi29 bacteriophage (2). Apical loop-apical loop known as 'kissing' complex triggers the dimerization of retroviral genomes (3) thanks to palindromic loop sequences. In prokaryotes many antisense RNAs make use of kissing interactions for recognizing their target mRNAs (4–7). Similar interactions were more recently demonstrated to play key roles in the organization of riboswitches (8,9) or in the substrate recognition by the *Neurospora* Varkud ribozyme (10).

The *in vitro* selection of aptamers against RNA hairpins leads also to oligonucleotides that recognize their target through loop–loop interactions (11–15). In the case of the RNA aptamer targeted to the TAR element of HIV-1 these interactions were demonstrated to be highly stable and specific due to a strong contribution of stacking interactions and to a network of hydrogen bonds (16).

Not every set of RNA hairpins with complementary loops generates stable kissing complexes (17,18). The stability of kissing complexes is highly dependent on the loop sequence and on the nature of loop closing residues (7,12,19,20). For instance inverting 5' to 3' the RNAI loop that mediates the formation of the RNAI-RNAII kissing complex modulating the ColE1 plasmid copy number results in 350-fold difference in the binding constant (21,22). It was also demonstrated that not all self-complementary loop sequences promote the dimerization of retroviral genomes (17). In the perspective of using RNA hairpins as modules for engineering biosensors or for build-

---

ing nanoscaffolds it is of interest to have in hands several kissing motifs. To this end we undertook the identification of a kissing repertoire within a randomly synthesized pool of RNA hairpins. In the present work we then used some sequences prone to stable loop–loop interactions for designing kissing aptamer-based sensors allowing the simultaneous detection of several molecules.

A huge number of technologies based on enzymatic and bioaffinity elements have been described for the detection of analytes such as biomarkers, hormones or pollutants in complex matrices (23,24). In order to meet the growing need for both high-throughput analysis and multi-target sensing in parallel, numerous research efforts have been concentrated on the development of platforms that fulfil real-time detection, improved specificity and multiplexing criteria. Significant advances have been reported in the multiplexed immunoanalysis area through the development of array and microbead assays (see for instance (25)). However, these platforms suffer from inherent drawbacks related to the low-throughput process for the antibody generation, the problem of batch-to-batch reproducibility and the difficulty to conjugate antibodies to labels or surfaces in a precisely defined manner. In addition, sandwich-like format allowing high specificity and facilitated signal translation is typically unattainable for the sensing of small targets.

Nucleic acid aptamers have received a great deal of attention in recent times as a promising class of bioaffinity reagents offering an alternative to antibodies (26–28). They are obtained by chemical means with a very high degree of reproducibility, leading to a reliable use in bioanalysis. Furthermore, they can be easily engineered and precisely functionalized to adapt to various sensor formats and transduction modes. Recent reports have described the use of multiple aptamers integrated in devices for analytical purposes. Most of them were dedicated to the simultaneous detection of proteins, cells or bacteria (29–31,32–35). Some examples of multiplexed analysis for small analytes were also reported but they are based on either competitive assays (36–42) or approaches of limited general applicability (43,44).

For analytical purposes particular attention is paid to aptamers that take advantage of a conformational change upon binding to the target molecule. Different designs were described that involve a monomolecular (45), a bimolecular (46) or even a trimolecular architecture (47) that ultimately translates binding into a signal, fluorescence energy transfer for instance. We recently described a new type of aptasensor relying on loop–loop (kissing) interactions (48,49): the binding of the ligand to an imperfect RNA hairpin aptamer named aptaswitch specifically triggers the formation of a kissing complex with a second RNA stem-loop termed aptakiss. This concept can be extended to the simultaneous detection of several molecules as far as specific aptaswitches are available for each of them on the one hand and several kissing sequences are identified on the other hand. We report here the design and the characterization of aptaswitch–aptakiss biosensors signalling the presence of purine derivatives through either surface plasmon resonance (SPR) or fluorescence anisotropy (FA) measurements.

MATERIALS AND METHODS

Oligonucleotides

The first RNA hairpin library (A) used for selection was constituted of two sub-pools, containing either 10 or 11 random nucleotides flanked by fixed regions:

5′GGUUACCAGCCUUCAC<u>UGCUCG</u>-N10/11-<u>CGAGCA</u>CCACGGUCGGUCACAC, where N can be anyone of the four standard ribonucleotides. Underlined sequences are complementary to each other thus generating a double-stranded stem. For the selection experiments with the enriched motif CCNY or RNGG, two other libraries, (B) 5′GGUUACCAGCCUUCAC<u>UGCUCG</u>NCCNYN<u>CGAGCA</u>CCACGGUCGGUCACAC and (C) 5′GGGAGGACGAAGCGG<u>ACGAGC</u>NRNGGNG<u>CUCGUC</u>AGAAGACACGCCCGA were used, respectively. Primers P20 5′GTGTGACCGACCGTGGTGC complementary to the 3′ end of the libraries A and B and 3′SL displaying the same polarity as the RNA pool and containing the T7 transcription promoter (underlined) 5′<u>TAATACGACTCACTATAG</u>GTTACCAGCCTTCACTGC were used for PCR amplifcation. Primers P1A 5′<u>TAATACGACTCACTATAG</u>GGAGGACGAAGCGG and P2A 5′TCGGGCGTGTCTTCTG were used for handling library C. The pools of random oligonucleotides and the different RNA aptamers were chemically synthesized in our laboratory on an Expedite 8909 synthesizer (Applied Biosystems) (Supplementary Figure S1). All oligonucleotides and transcription products were purified by electrophoresis on denaturing 20% polyacrylamide, 7M urea gels.

In vitro selection

The RNA library (50 picomoles) was labelled with [γ^{32}P]ATP (10 mCi/ml) (4500 Ci/mmol) from ICN Pharmaceutical, and kept at room temperature in a final volume of 10 μl of R buffer (20 mM HEPES, 20 mM sodium acetate, 140 mM potassium acetate and 3 mM magnesium acetate, pH 7.4) for 24 h. In subsequent selection rounds, in order to promote the selection of highly stable complexes, the RNA hairpin concentration was decreased 10 times at every round. Moreover, the incubation time was decreased from round to round (24 h for round 1, 6 h for round 2, 1 h for round 3 and 10 min for the final round). The RNA population was analysed by electrophoresis on a native gel (15% [w/v], 75:1 acrylamide:*bis*-acrylamide) in 50 mM Tris-acetate (pH 7.3 at 20°C) and 3 mM magnesium acetate (TAC buffer) at 100 V and 4°C for 15 h. The bands were visualized and quantified by Instant Imager (Packard Instrument). The bands corresponding to low mobility material were extracted from the gel, eluted for 16 h at 4°C, in 600 μl of the elution buffer (10 mM Tris-HCl, pH 7.4, 1 mM ethylenediaminetetraacetic acid (EDTA) and 25 mM NaCl) and then ethanol precipitated.

A second set of *in vitro* selection was performed using two RNA hairpin libraries displaying either 5′NCCNYN (library B) or 5′NRNGGN (library C) degenerated loop sequences. The two types of hairpins had different stems for preventing the formation of extended duplexes. Biotinylated candidates from library C were immobilized on streptavidin

MagneSphere paramagnetic particles from Promega and mixed with library B previously counter-selected against naked streptavidin beads. Two SELEX rounds were carried out with 50 nM and 5 nM of candidates, respectively. The bound candidates B were eluted from the beads by heating for 45 s at 85°C in 50 μl of water. In order to identify kissing partners of B hairpins in the C pool, the selection was carried out with immobilized B candidates. To this end the amplification of captured B candidates was performed with a 5′ oligo(dT) extended P20 primer. PCR products were therefore *in vitro* transcribed into oligo(A)-tailed RNA candidates. Oligo(A)-RNA B hairpins were captured on biotinylated oligo(dT) streptavidin beads. So, selection of candidates from library C was carried out against the immobilized selected oligo(A)-candidates from Library C.

RNA amplification, cloning and sequencing

Extracted RNA hairpins were denatured at 95°C for 40 s and placed on ice for 2 min. Then, the RNA pool was copied into cDNA using five units of the EZrTth (Perkin Elmer) polymerase at 63°C for 30 min according to the manufacturer's procedure. The candidates were amplified in the same tube containing the EZrTth buffer in addition to 300 μM of dNTP, 25 mM of MnOAc and 2 μM of each primer. Then, the reaction mixture was denatured at 94°C for 2 min and subjected to repeated cycles: 94°C for 1 min, 63°C for 1 min, for 40 cycles and 63°C for 7 min, for one final cycle. RNA hairpins were obtained by *in vitro* transcription, after precipitation of the PCR products with the Ampliscribe T7 high yield transcription kit from TEBU including [α ^{32}P]UTP (10 mCi/ml) (4500 Ci/mmol) from ICN Pharmaceuticals. The transcription products were purified by electrophoresis on 20% denaturing polyacrylamide gels and then used for the next selection cycle. Selected sequences from either the first or the second selection procedure were cloned using the TOPO TA cloning kit from Invitrogen and sequenced by using the dRhodamine Terminator Cycle sequencing kit from Perkin-Elmer, according to the manufacturers' instructions. The EMBOSS matcher based on Bill Pearson's align application was used to identify similarities in the selected hairpins.

Electrophoretic mobility shift assay

Equilibrium dissociation constant (K_D) of loop–loop RNA complexes was determined using electrophoretic mobility shift assay. In general, 0.1 or 1 nM of ^{32}P 5′ end-labelled hairpin was incubated with increasing concentrations of partners for 20 min at 23°C in 10 μl of R buffer. Binding reactions were loaded onto a non denaturing gel [12% (wt/v) 19:1 acrylamide/bis(acrylamide) in 50 mM Tris-acetate (pH 7.3 at 20°C) and 3 mM magnesium acetate) equilibrated at 4°C and electrophoresed overnight at 120 V (6 V/cm). Complexes were quantified by Instant Imager analysis (Hewlett-Packard). K_D values were deduced from data point fitting with Kaleidagraph 3.0 (Abelbeck software), according to the equation: $B = (Bmax)([L]_0) / ([L]_0 + K_D)$, where B is the proportion of complex, Bmax the maximum of complex formed and $[L]_0$ the total concentration of unlabelled ligand.

Surface plasmon resonance kinetic measurements

SPR experiments were performed on a BIAcore 2000 or 3000 apparatus (Biacore AB, Sweden) running with the BIAcore 2.1 software. Biotinylated RNA hairpins were immobilized at 40 nM (150–1000 RU), at a flow rate of 5 μl/min on streptavidin (SA) sensorchips in a 10 mM KH$_2$PO$_4$ buffer pH 6.2, containing 200 mM KCl, 10 mM MgCl$_2$ (M buffer) according to the procedure described in the BIA applications handbook. One streptavidin-coated flow-cell was used as a control: the signal from this control channel served as base line and was substracted to the RU change observed when complexes were formed. All partners were prepared in the above buffer at different concentrations (depending on the aptaswitch) and injected at a flow rate of 20 μl/min during 300 s. The sensorship surface was successfully regenerated with two 20 μl pulses of 3 mM EDTA, followed by one 20 μl pulse of distilled water and finally one 20 μl pulse of M buffer. Non linear regression analysis of single sensorgrams at, at least, five injected RNAs concentrations at 23°C was used to determine the kinetic parameters of the complex formation. The data were analysed with the BIA evaluation 2.2.4 software, assuming a pseudo-first order model, according to Equations (1) and (2), for the association and dissociation phases, respectively, where R is the signal response, Rmax the maximum response level, C is the molar concentration of the injected RNA molecule, k_{on} is the association rate constant and k_{off} is the dissociation rate constant.

$$\mathrm{d}R/\mathrm{d}t = k_{on} C (R\max - R) - k_{off} R \qquad (1)$$

$$\mathrm{d}R/\mathrm{d}t = -k_{off} R \qquad (2)$$

Fluorescence anisotropy (FA) assay

The binding buffer for FA assays previously optimized for ADOsw1 assay consisted in 10 mM Tris, pH 7.5, 100 mM NaCl, 10 mM MgCl$_2$ buffer (48). The oligonucleotide stock solutions were prepared in PCR water at 10 μM and stored at −20°C. For multiplex analyses, premixed working solutions of aptaswitches (ADOsw1' and THEsw4') or aptakisses (K1-fluorescein and K4-Texas red conjugates) were prepared from the individual stock solutions by 2.5-fold dilution with concentrated binding buffer. Aptakiss or aptaswitch solutions for controls were prepared individually in the same way.

The oligonucleotides working solutions were heated at 80°C for 5 min and then cooled and left at 4°C during 30 min in order to reach equilibrium prior to use. The ligand solutions (adenosine or theophylline) were prepared alone or with 500 μM of the other ligand in water. For dose response curves, the ligand concentration ranged from 0 to 500 μM. All solutions were filtered before use through 0.20 μm membrane filters.

To establish the dose response curves, aptakiss conjugates in the absence or in the presence of aptaswitches (10 nM final concentration for each oligonucleotide) were mixed with ligand solutions and placed into individual wells of black, 96-well Greiner Bio-One microplates. After 15 min of incubation at 4°C in dark the FA was measured on a Tecan Infinite F500 microplate reader (Männedorf, Switzerland) with

the plates filled with 100 μl of the mixture per well (triplicate experiments). Blank wells were filled with 100 μl of the 1× binding buffer.

Excitation was set at 485 ± 20 nm or 585 ± 20 nm and emission was collected with 535 ± 25 nm or 635 ± 30 nm bandpass filters for the Fluorescein or Texas Red probes, respectively.

The FA (r) was calculated by the instrument software, as classically reported:

$$r = \frac{I_{vv} - GI_{vh}}{I_{vv} + 2GI_{vh}} \quad (3)$$

where I_{vv} and I_{vh} are the vertically and horizontally polarized components of the emission after excitation by vertically polarized light. The instrumental correction factor G was determined according to the manufacturer's instructions.

The relative parameter Δr was calculated as follows:

$$\Delta r = r - r_0 \quad (4)$$

where r is the FA of the aptakiss in the presence of the aptaswitch and the target, r_0 is the FA in the absence of the target.

RESULTS AND DISCUSSION

Kissing repertoire

In order to get access to kissing-prone sequences we tailored an experiment (Figure 1A) using a synthetic library of RNA hairpins with an identical six base pair stem and a random loop sequence, either 10 or 11 nucleotides long (Figure 1B). This pool displays a complexity of ∼5.2 × 10^6 candidates. For some candidates the first and last nucleotides of the random region will be complementary to each other thus potentially extending the double-stranded stem and consequently reducing the loop size. Therefore our library will contain every loop with an even or odd number of residues up to 11 with variable loop closing bases.

^{32}P 5′ end-labelled candidates constituting this pool loaded on a non-denaturing polyacrylamide gel showed two bands (Figure 1C). The fast migrating band corresponds to hairpin monomers whereas the slow migrating one corresponds to RNA–RNA complexes that might include kissing ones. Material from this band was extracted from the gel and following treatment and transcription (see 'Materials and Methods') was reloaded on a new non-denaturing gel. After four rounds of selection-amplification carried out at decreasing oligonucleotide concentration, the RNA contained in the slow band amounted to 54% compared to 18% at the first step (not shown).

Following cloning and sequencing of the fourth pool constituting the slow migrating band we analysed 110 candidates that were all predicted to form hairpins as expected, some of them with an imperfect stem in the top part corresponding to the 5′ and 3′ ends of the random region. In addition some candidates exhibited a shorter random window likely due to polymerase mistakes. Sequences were classified into 45 families of at least three sequences displaying partial loop complementarity over at least five contiguous bases with one of the 110 candidates; as an example six of these families, a to f, are shown in Figure 2. A seventh family (g) is composed of palindromic sequences for which three representatives are given (Figure 2).

We then evaluated the binding characteristics of potential complexes from each of the 45 families by electrophoretic mobility shift of a ^{32}P labelled hairpin in the presence of two different concentrations (10 and 200 nM) of the unlabelled putative partner. For instance, in the f family we identified both strong (K78) and weak (K41, K14) binders (Figure 3A). Using this screen we determined that seven couples and three palindromic sequences displayed an affinity stronger than 10 nM (i.e. displayed a profile with more than 50% of the material in the retarded band at the lowest concentration) and 21 combinations had an affinity between 10 and 200 nM. Titration experiment of ^{32}P-labelled K24 by K78 led to a K_D of 0.42 ± 0.05 nM (Figure 3B and C).
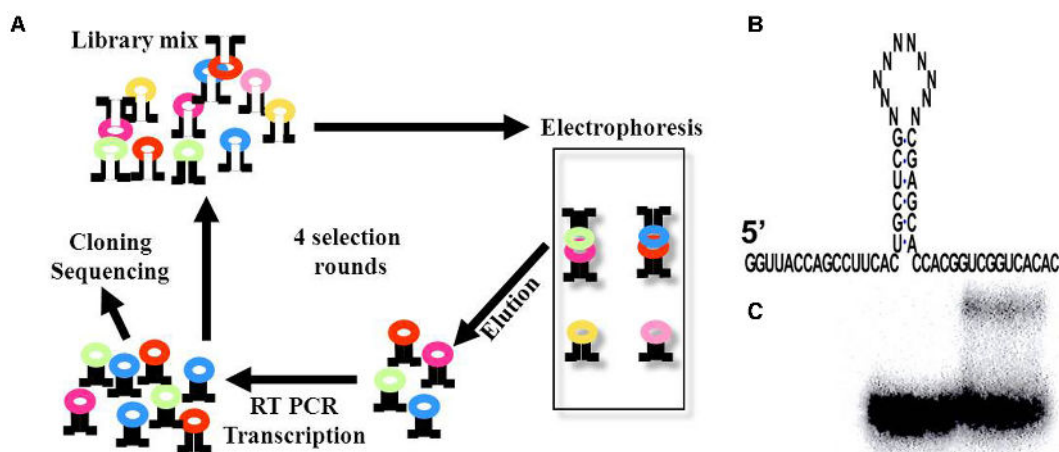

Figure 1. Identification of kissing RNA hairpins from a randomly synthesized library (**A**) scheme of the selection procedure: the pool of RNA hairpins is loaded on a non-denaturing polyacrylamide gel. The slowly migrating material is extracted, amplified and reloaded on a new gel. After four successive rounds of electrophoretic separation and amplification, candidates are cloned and sequenced. (**B**) schematic secondary structure of the library. N can be any of the four nucleotides A, U, G or C. Pools were prepared with N = 10 or N = 11 and mixed prior to selection. (**C**) gel electrophoresis analysis of the hairpin pool at the first round either heat-denatured prior to loading (left lane) or without denaturation (right lane).

Figure 2. Sequences of selected kissing loops and binding properties of candidate hairpins. For the six listed families a to f, putative partners (5′ to 3′ from left to right) are aligned against one given sequence (top line of each family; 3′ to 5′ left to right). Families a, b, c, e and f display the 5′CCNY motif (boxed) whereas family d contains the 5′RYRY motif (boxed). The potential complementary sequence of the putative kissing partner is shown in light grey. The g family is composed of palindromic motifs (light grey). The formation of G.U pairs was tolerated. K_D values (nM), estimated by EMSA as indicated in the text, are given to the right. ND = not determined.

Members of the strong binder sub-population characterized by an evaluated K_D below 10 nM, displayed at least four non-contiguous GC pairs in the kissing motif; actually for these candidates the GC content of the putative loop–loop helix is 76% in fair agreement with previous results on the dimerization element of the HIV-1 genome (18). Loop comparison of strong binders led to the identification of a 4 nucleotide loop–loop consensus motif: 5′CCNY where N is A, U, C or G or its complement 5′RNGG. 52% of the sequences in the pool of the 110 selected candidates possessed either a 5′CCNY or a 5′RNGG motif (Supplementary Figure S2). Eight couples shown in Figure 2 display a 6 nucleotide long putative Watson Crick loop–loop he-

lix whereas five combinations show perfect complementarity over 5 or 7 nucleotides. This suggests that longer complementary regions do not provide additional stability. Indeed, increasing the size of the loop–loop helix requires a longer linker for spanning the distance between 5′ and 3′ ends of this helix across the groove. Another frequently encountered motif RYRY alternates pyrimidines and purines (Supplementary Figure S3). This second class was not further characterized.

Nucleic acid bases closing the loop sequence were shown to play a key role for the stability of kissing complexes. For instance, in the case of the anti-TAR aptamer a closing G-A combination accounts for its high affinity for the TAR hairpin (12). In order to determine the best residues flanking the CCNY/RNGG motifs and to identify the preferred central residue we carried out a second *in vitro* selection using hairpin libraries with a 6 nucleotide loop randomized at three positions each, in addition to the degenerated Y or R residue: 5′UGCUCGNCCNYNCGAGCA and 5′ACGAGCNRNGGNGCUCGU, N being anyone of the four residues A, U, G or C. Two selection rounds were performed according to the procedure described in the 'Materials and Methods'. Eighty-eight and 86 candidates containing either CCNY or RNGG were sequenced, respectively. K1 (5′UGCUCGGCCCCGCGAGCA) and K1′ (5′ ACGAGCUGGGGCGCUCGU) were the most represented candidates accounting for 18.5 and 11.5% of all sequences, respectively. G was by far the most frequent base at the first and last positions for both the NCC-NYN and NRNGGN motifs with scores ranging from 38 to 53% (Supplementary Figure S4). Purine–purine combinations for the closing residues were over represented and amounted to 45 and 36% for the NCCNYN and NRNGGN motifs, respectively, in fair agreement with previous results (50). In addition the central N position of the kissing motifs revealed a slight enrichment (33%) in G residues for CCNY and a marked preference for G in the case of RNGG. Altogether G is highly favoured in this kissing determinant as it accounts for ∼80 and 50% of the R and N position, respectively (Supplementary Figure S4). The potential for G to pair either with C or U adds one more possibility for G being selected. When GU pairs are tolerated 12% of the kissing motifs contain GU in the central region. GU combination appears with a low frequency (8%) at the positions adjacent to the stem but might play a key role.

Characterization of kissing complexes by surface plasmon resonance

In the perspective of their use in biosensing devices we then undertook the characterization of four kissing combinations K1–K1' to K4–K4' (see Supplementary Figure S1 for sequences) taking advantage of both the above selection and previously characterized RNA–RNA kissing complexes (11,13–15,50). K1 belongs to the CCNY class whereas K2 displays both CCNY and YRYR motifs. Both K1 and K2 were identified through the selection process described above. In contrast, K3 corresponds to the top part of the TAR RNA element of HIV-1 that we previously demonstrated to engage a strong kissing interaction
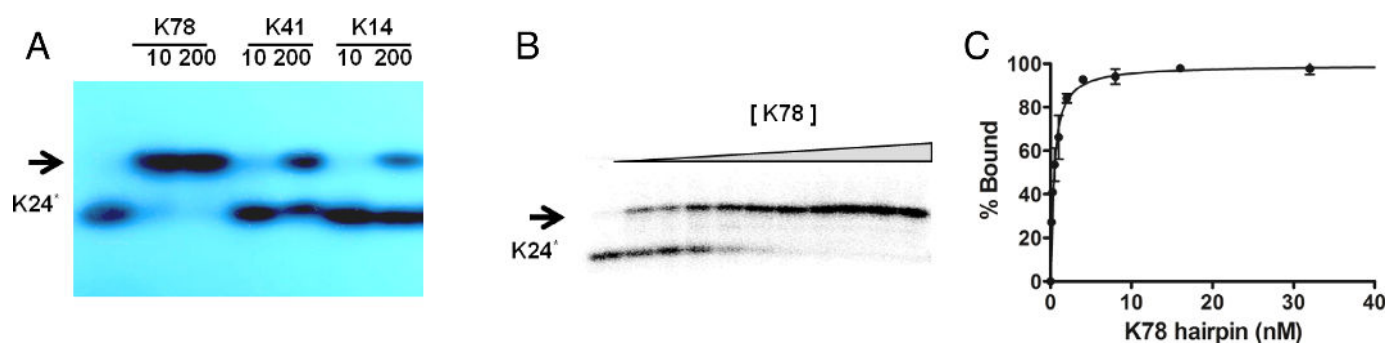
Figure 3. Gel electrophoresis analysis of kissing complexes. (**A**) ^{32}P-labelled candidate K24* was loaded in the absence (left lane) or in the presence of the putative partner K78, K41or K14 at either 10 or 200 nM, as indicated at the top of the lanes. The arrow (left) indicates the position of the kissing complex. (**B**) Gel electrophoresis analysis of the titration of ^{32}P-labelled K24* by K78. K78 concentration was increased from 0 (left lane) to 62.5 nM (right lane). (**C**) Quantitative analysis of electrophoretic band-shift assay (see 'Materials and Methods').

with a hairpin aptamer (12,50–52). K4 that contains the RYRY motif is the top part of the pre-miRNA let7b (53) against which we recently identified a kissing aptamer (unpublished). RNA hairpins K1' to K4' with loops complementary to that of K1 to K4, respectively, were prepared, the kissing motif being displayed in the context of a hairpin with a 6 or 7 nucleotide loop (Supplementary Figure S4). Hairpins K1 to K4 were chemically synthesized with a 3' biotinyl residue.

We investigated by SPR the properties of the four preselected kissing complexes by immobilizing the biotinylated hairpins K1 to K4 on different channels of a streptavidin sensor chip. Individual solutions of K1', K2', K3' or K4' were flown over the chip. A nice resonance signal was obtained as expected for each cognate combination K1-K1' to K4-K4', respectively. K_D values were determined by SPR to be in the low nanomolar range: 6.9 +/− 1.1 nM, 17 +/−3 nM, 2.9 +/− 0.3 nM for K1-K1' (48), K3-K3' (12) and K4-K4', respectively. The sensorgrams obtained for K2-K2' did not allow the accurate determination of the K_D. In contrast no signal was observed for any other combination (Supplementary Figure S5) except K1–K3' (not shown); consequently we no longer used the K3–K3' complex and restricted further investigations to the three other combinations that do not generate cross interactions for the design of kissing complex-based aptasensors.

Converting aptamers to GTP, adenosine and theophylline into aptaswitches

We extended the aptaswitch–aptakiss concept recently described (48) to the simultaneous detection of several molecules. We took advantage of previously characterized aptamers for the design of specific aptaswitches. Indeed aptamers organized as imperfect hairpins whose apical loop is not involved in the binding of their ligand can potentially be converted into aptaswitches, i.e. oligonucleotides that change conformation upon association with their cognate target molecule. To this end we first substituted a short sequence prone to kissing interaction to the original aptamer apical loop. We introduced loops of K1', K2' or K4' in aptamers previously selected against adenosine (54), GTP (55) or theophylline (56), thus generating ADOsw1', GTPsw2' and THEsw4', respectively (Figure 4 and Supple-
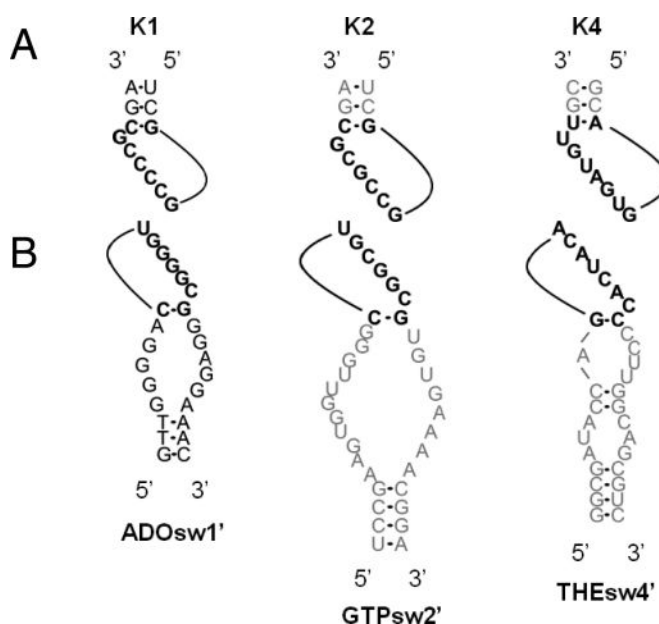

Figure 4. Predicted secondary structures (**A**) of aptakiss K1, K2 and K4 and (**B**) of aptaswitch ADOsw1'specific for adenosine, GTPsw2' for GTP and THEsw4' for theophylline. Only the top part of the aptakisses is shown; see Supplementary Figure S1 for full-length sequences. Bold letters indicate the kissing motifs.

mentary Figure S1). These aptamers are characterized by a purine-rich internal loop that constitutes the binding site of their ligand. We tailored the short double-stranded regions above and below the central loop in such a way that the aptaswitch conditionally folds into a hairpin, upon addition of the cognate target molecule. We thus left a single G–C or C–G pair potentially closing the apical loop (Figure 4). The aptaswitch ADOsw1' was previously characterized: a specific and concentration-dependent SPR or fluorescence signal was observed upon the simultaneous addition of adenosine and K1 whereas no signal was detected in the presence of inosine that does not bind to the parent aptamer (48). GTPsw2' is derived from the GTP RNA aptamer (55) by subsituting the K2' motif to the parent apical loop (Figure 4). Its specific responsiveness to GTP is retained: a concentration-dependent SPR signal was observed
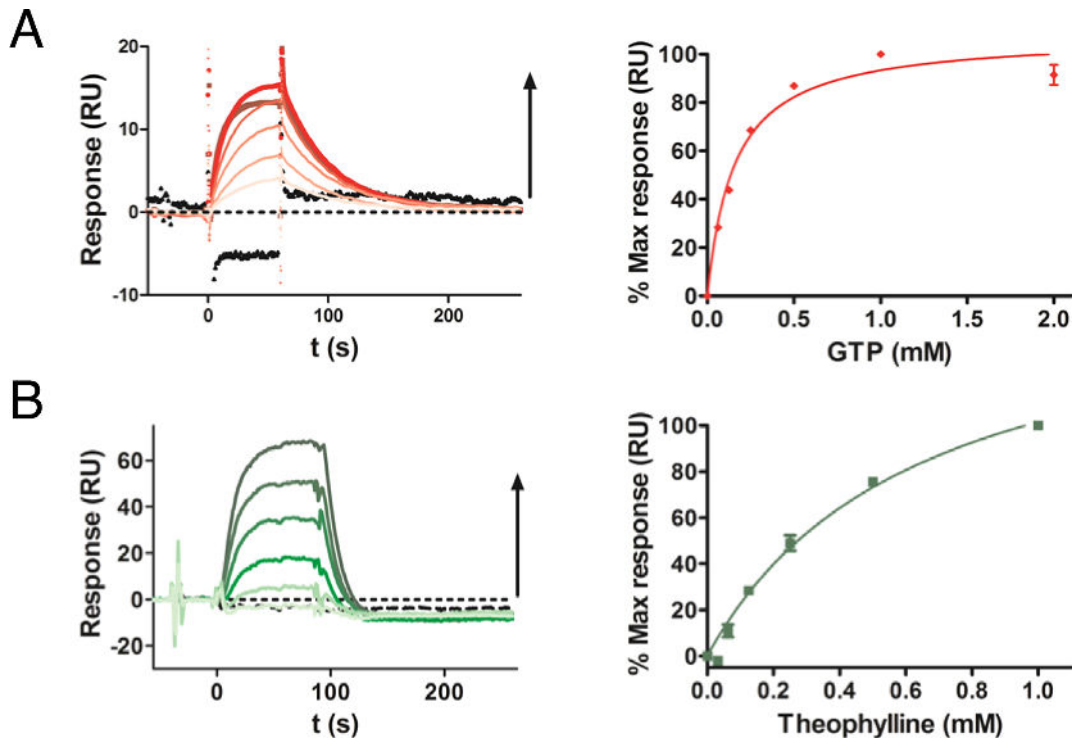
Figure 5. SPR analysis of aptaswitch–aptakiss complexes. (**A**) Left: Biotinylated K2 was immobilized on the biochip. A mixture of 5 μM GTPsw2' with either GTP at a concentration between 60 and 2000 μM (red curves) or 2000 μM ATP (black line) was injected. Right: The maximum resonance signal from sensorgrams is plotted against the GTP concentration. (**B**) Left: Biotinylated K4 was immobilized on the biochip. A mixture of 1 μM THEsw4' with either theophylline at the concentration between 30 and 1000 μM (green curves) or 1000 μM caffeine (black line) was injected. Right: The maximum resonance signal from sensorgrams is plotted against the theophylline concentration. Results in (A) and (B) right are expressed as a mean ± SEM of two independent experiments. Dotted lines in left panels of (A) and (B) correspond to the injection of the buffer. Experiments were carried out in a 10 mM KH_2PO_4 buffer pH 6.2, containing 200 mM KCl, 10 mM $MgCl_2$ at room temperature (see 'Materials and Methods' for details).
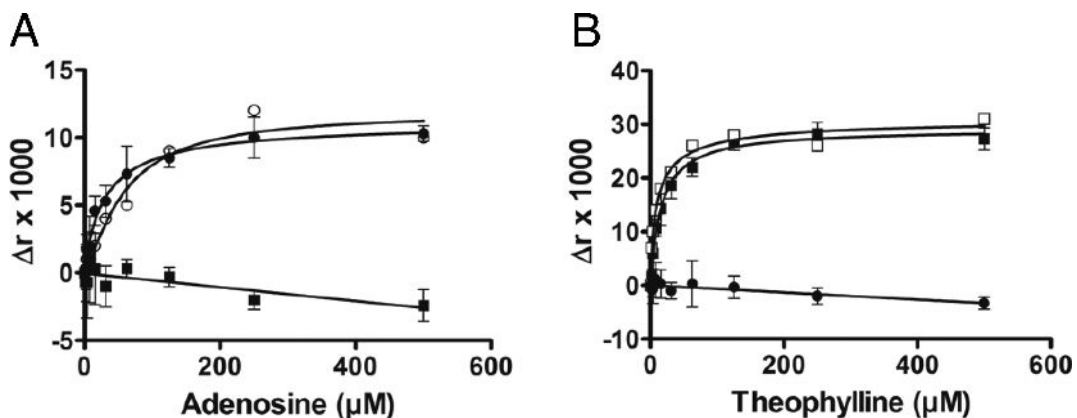

Figure 6. Multicolour FA detection of aptaswitch–aptakiss complexes. (**A**) Increasing amounts of adenosine were added to a mixture of THEsw4', ADOsw1', K4-TR and K1-F (10 nM each). FA was measured for each concentration (λ_{Em} = 535 nm, fluorescein reporter, black circles or 635 nm, Texas red reporter, black squares). The control contained only ADOsw1', K1-F and adenosine (λ_{Em} = 535 nm, fluorescein reporter, empty circles). Measurements were carried out in a 10 mM Tris-HCl, pH 7.5 buffer containing 100 mM NaCl and 10 mM $MgCl_2$ at 4°C. (**B**) Increasing amounts of theophylline were added to a mixture of THEsw4', ADOsw1', K4-TR and K1-F. Emission wavelength (λ_{Em}) was set at 635 nm (Texas red reporter, black squares) or 535 nm (fluorescein reporter, black circles). Control contained only THEsw4', K4-TR and theophylline (empty squares; λ_{Em} = 635 nm).

in the presence of K2 upon addition of GTP whereas no resonance was seen with ATP (Figure 5A). A mixture of the aptaswitch THEsw4' (Figure 4) and of theophylline induces a SPR signal when flown over a chip on which K4 was immobilized (Figure 5B). No signal was detected in the presence of caffeine indicating that the specificity of the parent aptamer is retained. However, the affinity of THEsw4' for theophylline is significantly reduced compared to the parent aptamer (56). It should be pointed out that the three aptaswitch–aptakiss complexes were evaluated under the same ionic conditions, a prerequisite for multiplex analysis, even though this does not correspond to the medium in which parent aptamers were selected.

Simultaneous detection of ligands by surface plasmon resonance

To this end we used a SPR streptavidin biochip with four channels. Biotinylated aptakiss K1, K2 and K4 were immobilized on channels 1, 2 and 3, respectively, the fourth one being used for control. As shown (Supplementary Figure S6) flowing ADOsw1', GTPsw2' or THEsw4' with saturating concentrations of the cognate ligand, adenosine, GTP or theophylline, respectively, resulted in a signal exclusively on the corresponding functionalized channel, i.e. 1, 2 or 3, respectively. More complex mixtures were then tested. The simultaneous presence of the three aptaswitches allowed the specific detection of one ligand: for instance, theophylline in the presence of ADOsw1'+ GTPsw2'+ THEsw4' yielded a signal exclusively on channel 3 (Supplementary Figure S7a). Similar results were obtained for adenosine and GTP. The mixture with one aptaswitch and three ligands also generated a specific response: for instance, GTPsw2' supplemented with adenosine, GTP and theophylline gave a signal only on channel 2 (Supplementary Figure S7b). The use of either ADOsw1' or THEsw4' with the three ligands also allowed the detection of the cognate ligand.

Simultaneous detection of adenosine and theophylline by multicolour fluorescence anisotropy system

Multiplexing is of higher interest if performed in solution. The association of the aptakiss to the ligand-aptaswitch complex results in reduced mobility of the aptakiss and consequently in an increased FA signal. We used this method for the simultaneous detection of our ligands. However, as guanine induces strong quenching of many fluorophores (57), we restricted the assay to the simultaneous detection of adenosine and theophylline. We synthesized 3′ fluorescein-conjugated K1 (K1-F) and 3′ Texas red-conjugated K4 (K4-TR) (Supplementary Figure S1). K4-TR was truncated compared to the original K4 aptakiss in order to enhance the FA change upon binding to the folded THEsw4'. These dyes display a limited spectral overlap allowing their simultaneous monitoring. The addition of THEsw4' to a solution of K4-TR at increasing concentration of theophylline led to a specific concentration-dependent increased TR FA; no variation was observed in the presence of caffeine that is not recognized by the theophylline aptamer (Supplementary Figure S8). The effect was not altered by the presence of adenosine at concentrations up to 500 μM. In an attempt to mimic multicolour fluorescence detection we prepared a mixture of the two aptaswitches ADOsw1' and THEsw4' with the two fluorescent aptakiss conjugates. A dose-dependent increase of FA for K4-TR was observed upon addition of theophylline whereas no FA variation could be detected for the fluorescein probe (Figure 6A). Conversely, the addition of adenosine to the dual reporter system induced a FA increase for K1-F only (Figure 6B). Moreover, we found that the limits of detection (based on 3σ) for the multiplexed system (4 μM for theophylline and 10 μM for adenosine) were comparable to those determined for the individual aptasensors.

CONCLUSION

The analysis of a pool comprising $\sim 5 \times 10^6$ hairpins led us to identify more than 50 loop sequences, prone to the formation of kissing complexes characterized by a K_D in the low-to-medium nanomolar range. For the large majority of the kissing loops the complementarity extends to 6 or 7 nucleotides, a value that is frequently encountered for antisense RNA loops involved in natural loop–loop complexes (7,58) and for retroviral dimerization motifs (59). Our criteria for the identification of stable kissing complexes did not allow the identification of every possibility. We obviously missed all kissing combinations with a number of loop–loop base pairs lower than 5; indeed some kissing complexes were reported to engage as few as two base pairs (60). However, our screening allowed the identification of kissing signatures CCNY and RYRY in addition to the YUNR sequence that was reported previously (7,58).

The specificity of the loop–loop interaction as well as the stability of kissing complexes offers many possibilities for designing tools and devices of biotechnological interest. In the present study kissing sequences were introduced in the apical loop of switching aptamers leading to the design of sensors for the simultaneous detection of three different ligands as loop–loop complexes are much more stable than complexes formed between a hairpin and a linear sequence (12,61). More targets could be envisaged as far as a specific signal is associated to each of them. In this respect other types of labels could be used such as quantum dots or electroactive labels. These conditional kissing interactions could also be of interest for the assembly of nanostructures. Work along these lines is under way in our laboratory.

SUPPLEMENTARY DATA

Supplementary Data are available at NAR Online.

REFERENCES

1. Ferrandon,D., Koch,I., Westof,E. and Nusslein-Volhard,C. (1997) RNA-RNA interaction is required for the formation of specific bicoid mRNA 3'UTR-STAUFEN ribonucleoproteic particles. *EMBO J.*, **16**, 1751–1758.

2. Xiao,F., Zhang,H. and Guo,P. (2008) Novel mechanism of hexamer ring assembly in protein/RNA interactions revealed by single molecule imaging. *Nucleic Acids Res.*, **36**, 6620–6632.

3. Paillart,J.C., Skripkin,E., Ehresmann,B., Ehresmann,C. and Marquet,R. (1996) A loop-loop 'kissing' complex is the essential part of the dimer linkage of genomic HIV-1 RNA. *Proc. Natl Acad. Sci. U.S.A.*, **93**, 5572–5577.

4. Tomizawa,J.I. (1986) Control of ColE1 plasmid replication: binding of RNA I to RNA II and inhibition of primer formation. *Cell*, **47**, 89–97.

5. Persson,C., Wagner,E.G.H. and Nordström,K. (1990) Control of replication of plasmid R1: structures and sequences of the antisense RNA, CopA, required for its binding to the target RNA, CopT. *EMBO J.*, **9**, 3761–3775.

6. Argaman,L. and Altuvia,S. (2000) fhlA repression by OxyS RNA: kissing complex formation at two sites results in a stable antisense-target RNA complex. *J. Mol. Biol.*, **300**, 1101–1112.

7. Brunel,C., Marquet,R., Romby,P. and Ehresmann,C. (2002) RNA loop-loop interactions as dynamic functional motifs. *Biochimie*, **84**, 925–944.

8. Holmstrom,E.D., Polaski,J.T., Batey,R.T. and Nesbitt,D.J. (2014) Single-molecule conformational dynamics of a biologically functional hydroxocobalamin riboswitch. *J. Am. Chem. Soc.*, **136**, 16832–16843.

9. Allner,O., Nilsson,L. and Villa,A. (2013) Loop-loop interaction in an adenine-sensing riboswitch: a molecular dynamics study. *RNA*, **19**, 916–926.

10. Bouchard,P. and Legault,P. (2014) Structural insights into substrate recognition by the Neurospora Varkud satellite ribozyme: importance of U-turns at the kissing-loop junction. *Biochemistry*, **53**, 258–269.

11. Boiziau,C., Dausse,E., Yurchenko,L. and Toulmé,J.J. (1999) DNA aptamers selected against the HIV-1 TAR RNA element form RNA/DNA kissing complexes. *J. Biol. Chem.*, **274**, 12730–12737.

12. Ducongé,F., Di Primo,C. and Toulmé,J.J. (2000) Is a closing 'GA pair' a rule for stable loop-loop RNA complexes? *J. Biol. Chem.*, **275**, 21287–21294.

13. Aldaz-Carroll,L., Tallet,B., Dausse,E., Yurchenko,L. and Toulmé,J.J. (2002) Apical loop-internal loop interactions: a new RNA-RNA recognition motif identified through in vitro selection against RNA hairpins of the hepatitis C virus mRNA. *Biochemistry*, **41**, 5883–5893.

14. Kikuchi,K., Umehara,T., Fukuda,K., Hwang,J., Kuno,A., Hasegawa,T. and Nishikawa,S. (2003) RNA Aptamers Targeted to Domain II of Hepatitis C Virus IRES That Bind to Its Apical Loop Region. *J. Biochem. (Tokyo)*, **133**, 263–270.

15. Da Rocha Gomes,S., Dausse,E. and Toulmé,J.J. (2004) Determinants of apical loop-internal loop RNA-RNA interactions involving the HCV IRES. *Biochem. Biophys. Res. Commun.*, **322**, 820–826.

16. Van Melckebeke,H., Devany,M., Di Primo,C., Beaurain,F., Toulmé,J.J., Bryce,D.L. and Boisbouvier,J. (2008) Liquid-crystal NMR structure of HIV TAR RNA bound to its SELEX RNA aptamer reveals the origins of the high stability of the complex. *Proc. Natl Acad. Sci. U.S.A.*, **105**, 9210–9215.

17. Clever,J.L., Wong,M.L. and Parslow,T.G. (1996) Requirements for kissing-loop-mediated dimerization of human immunodeficiency virus RNA. *J. Virol.*, **70**, 5902–5908.

18. Lodmell,J.S., Ehresmann,C., Ehresmann,B. and Marquet,R. (2000) Convergence of natural and artificial evolution on an RNA loop-loop interaction: The HIV-1 dimerization initiation site. *RNA*, **6**, 1267–1276.

19. Paillart,J.C., Westhof,E., Ehresmann,C., Ehresmann,B. and Marquet,R. (1997) Non-canonical interactions in a kissing loop complex: the dimerization initiation site of HIV-1 genomic RNA. *J. Mol. Biol.*, **270**, 36–49.

20. Chen,A.A. and Garcia,A.E. (2012) Mechanism of enhanced mechanical stability of a minimal RNA kissing complex elucidated by nonequilibrium molecular dynamics simulations. *Proc. Natl Acad. Sci. U.S.A.*, **109**, E1530–E1539.

21. Eguchi,Y. and Tomizawa,J. (1990) Complex formed by complementary RNA stem-loops and its stabilization by a protein: function of CoIE1 Rom protein. *Cell*, **60**, 199–209.

22. Eguchi,Y. and Tomizawa,J. (1991) Complexes formed by complementary RNA stem-loops. Their formations, structures and interaction with ColE1 Rom protein. *J. Mol. Biol.*, **220**, 831–842.

23. Holzinger,M., Le Goff,A. and Cosnier,S. (2014) Nanomaterials for biosensing applications: a review. *Front. Chem.*, **2**, 63.

24. Bahadir,E.B. and Sezginturk,M.K. (2014) Electrochemical biosensors for hormone analyses. *Biosens. Bioelectron.*, **68C**, 62–71.

25. Pavkovic,M., Riefke,B., Gutberlet,K., Raschke,M. and Ellinger-Ziegelbauer,H. (2014) Comparison of the MesoScale Discovery and Luminex multiplex platforms for measurement of urinary biomarkers in a cisplatin rat kidney injury model. *J. Pharmacol. Toxicol. Methods*, **69**, 196–204.

26. Ma,H., Liu,J., Ali,M.M., Mahmood,M.A., Labanieh,L., Lu,M., Iqbal,S.M., Zhang,Q., Zhao,W. and Wan,Y. (2015) Nucleic acid aptamers in cancer research, diagnosis and therapy. *Chem. Soc. Rev.*, **44**, 1240–1256.

27. Mascini,M., Palchetti,I. and Tombelli,S. (2012) Nucleic acid and peptide aptamers: fundamentals and bioanalytical aspects. *Angew. Chem. Int. Ed. Engl.*, **51**, 1316–1332.

28. Mairal,T., Cengiz Ozalp,V., Lozano Sanchez,P., Mir,M., Katakis,I. and O'Sullivan,C.K. (2007) Aptamers: molecular tools for analytical applications. *Anal. Bioanal. Chem.*, **390**, 989–1007.

29. Lin,C., Liu,Y. and Yan,H. (2007) Self-assembled combinatorial encoding nanoarrays for multiplexed biosensing. *Nano Lett.*, **7**, 507–512.

30. Zhang,H., Li,X.F. and Le,X.C. (2008) Tunable aptamer capillary electrophoresis and its application to protein analysis. *J. Am. Chem. Soc.*, **130**, 34–35.

31. Gold,L., Ayers,D., Bertino,J., Bock,C., Bock,A., Brody,E.N., Carter,J., Dalby,A.B., Eaton,B.E., Fitzwater,T. *et al.* (2010) Aptamer-based multiplexed proteomic technology for biomarker discovery. *PLoS One*, **5**, e15004.

32. Rosman,C., Prasad,J., Neiser,A., Henkel,A., Edgar,J. and Sonnichsen,C. (2013) Multiplexed plasmon sensor for rapid label-free analyte detection. *Nano Lett.*, **13**, 3243–3247.

33. Zuo,P., Li,X., Dominguez,D.C. and Ye,B.C. (2013) A PDMS/paper/glass hybrid microfluidic biochip integrated with aptamer-functionalized graphene oxide nano-biosensors for one-step multiplexed pathogen detection. *Lab. Chip*, **13**, 3921–3928.

34. Zheng,F., Cheng,Y., Wang,J., Lu,J., Zhang,B., Zhao,Y. and Gu,Z. (2014) Aptamer-functionalized barcode particles for the capture and detection of multiple types of circulating tumor cells. *Adv. Mater.*, **26**, 7333–7338.

35. Liu,Y., Matharu,Z., Rahimian,A. and Revzin,A. (2015) Detecting multiple cell-secreted cytokines from the same aptamer-functionalized electrode. *Biosens. Bioelectron.*, **64**, 43–50.

36. Liu,J., Lee,J.H. and Lu,Y. (2007) Quantum dot encoding of aptamer-linked nanostructures for one-pot simultaneous detection of multiple analytes. *Anal. Chem.*, **79**, 4120–4125.

37. Zhang,J., Wang,L., Zhang,H., Boey,F., Song,S. and Fan,C. (2010) Aptamer-based multicolor fluorescent gold nanoprobes for multiplex detection in homogeneous solution. *Small*, **6**, 201–204.

38. Luo,F., Zheng,L., Chen,S., Cai,Q., Lin,Z., Qiu,B. and Chen,G. (2012) An aptamer-based fluorescence biosensor for multiplex detection using unmodified gold nanoparticles. *Chem. Commun. (Camb)*, **48**, 6387–6389.

39. Wang,L., Zhu,J., Han,L., Jin,L., Zhu,C., Wang,E. and Dong,S. (2012) Graphene-based aptamer logic gates and their application to multiplex detection. *ACS Nano*, **6**, 6659–6666.

40. Perrier,S., Zhu,Z., Fiore,E., Ravelet,C., Guieu,V. and Peyrin,E. (2014) Capillary gel electrophoresis-coupled aptamer enzymatic cleavage protection strategy for the simultaneous detection of multiple small analytes. *Anal. Chem.*, **86**, 4233–4240.

41. Wang,Y., Tang,L., Li,Z., Lin,Y. and Li,J. (2014) In situ simultaneous monitoring of ATP and GTP using a graphene oxide nanosheet-based sensing platform in living cells. *Nat. Protoc.*, **9**, 1944–1955.

42. Zhang,H., Hu,X. and Fu,X. (2014) Aptamer-based microfluidic beads array sensor for simultaneous detection of multiple analytes employing multienzyme-linked nanoparticle amplification and quantum dots labels. *Biosens. Bioelectron.*, **57**, 22–29.
43. Kim,Y.S. and Jurng,J. (2011) Gold nanoparticle-based homogeneous fluorescent aptasensor for multiplex detection. *Analyst*, **136**, 3720–3724.
44. Niu,S., Lv,Z., Liu,J., Bai,W., Yang,S. and Chen,A. (2014) Colorimetric aptasensor using unmodified gold nanoparticles for homogeneous multiplex detection. *PLoS One*, **9**, e109263.
45. Stojanovic,M.N., de Prada,P. and Landry,D.W. (2001) Aptamer-based folding fluorescent sensor for cocaine. *J. Am. Chem. Soc.*, **123**, 4928–4931.
46. Nutiu,R. and Li,Y. (2005) Aptamers with fluorescence-signaling properties. *Methods*, **37**, 16–25.
47. Nutiu,R. and Li,Y. (2003) Structure-switching signaling aptamers. *J. Am. Chem. Soc.*, **125**, 4771–4778.
48. Durand,G., Lisi,S., Ravelet,C., Dausse,E., Peyrin,E. and Toulme,J.J. (2014) Riboswitches based on kissing complexes for the detection of small ligands. *Angew. Chem. Int. Ed. Engl.*, **53**, 6942–6945.
49. Goux,E., Lisi,S., Ravelet,C., Durand,G., Fiore,E., Dausse,E., Toulme,J.J. and Peyrin,E. (2015) An improved design of the kissing complex-based aptasensor for the detection of adenosine. *Anal. Bioanal. Chem.*, **407**, 6515–6524.
50. Ducongé,F. and Toulmé,J.J. (1999) In vitro selection identifies key determinants for loop-loop interactions: RNA aptamers selective for the TAR RNA element of HIV-1. *RNA*, **5**, 1605–1614.
51. Boucard,D., Toulmé,J.J. and Di Primo,C. (2006) Bimodal loop-loop interactions increase the affinity of RNA aptamers for HIV-1 RNA structures. *Biochemistry*, **45**, 1518–1524.
52. Darfeuille,F., Reigadas,S., Hansen,J.B., Orum,H., Di Primo,C. and Toulme,J.J. (2006) Aptamers targeted to an RNA hairpin show improved specificity compared to that of complementary oligonucleotides. *Biochemistry*, **45**, 12076–12082.
53. Griffiths-Jones,S., Grocock,R.J., van Dongen,S., Bateman,A. and Enright,A.J. (2006) miRBase: microRNA sequences, targets and gene nomenclature. *Nucleic Acids Res.*, **34**, D140–D144.
54. Davis,J.H. and Szostak,J.W. (2002) Isolation of high-affinity GTP aptamers from partially structured RNA libraries. *Proc. Natl Acad. Sci. U.S.A.*, **99**, 11616–11621.
55. Huizenga,D.E. and Szostak,J.W. (1995) A DNA aptamer that binds adenosine and ATP. *Biochemistry*, **34**, 656–665.
56. Jenison,R.D., Gill,S.C., Pardi,A. and Polisky,B. (1994) High-resolution molecular discrimination by RNA. *Science*, **263**, 1425–1429.
57. Nazarenko,I., Pires,R., Lowe,B., Obaidy,M. and Rashtchian,A. (2002) Effect of primary and secondary structure of oligodeoxyribonucleotides on the fluorescent properties of conjugated dyes. *Nucleic Acids Res.*, **30**, 2089–2195.
58. Franch,T. and Gerdes,K. (2000) U-turns and regulatory RNAs. *Curr. Opin. Microbiol.*, **3**, 159–164.
59. Paillart,J.C., Marquet,R., Skripkin,E., Ehresmann,C. and Ehresmann,B. (1996) Dimerization of retroviral genomic RNAs: structural and functional implications. *Biochimie*, **78**, 639–653.
60. Kim,C.H. and Tinoco,I. Jr (2000) A retroviral RNA kissing complex containing only two G.C base pairs. *Proc. Natl Acad. Sci. U.S.A.*, **97**, 9396–9401.
61. Grosjean,H., Soll,D.G. and Crothers,D.M. (1976) Studies of the complex between transfer RNAs with complementary anticodons. I. Origins of enhanced affinity between complementary triplets. *J. Mol. Biol.*, **103**, 499–519.